nature nanotechnology

SUPPLEMENTARY INFORMATION

DOI: 10.1038/NNANO.2015.207

Evolution of a designless nanoparticle network into reconfigurable Boolean logic

Authors: S.K. Bose, C.P. Lawrence, Z. Liu, K.S. Makarenko, R.M.J. van Damme, H.J. Broersma and W.G. van der Wiel

S1. Nanoparticle network characteristics

Charging energy estimation

The self-capacitance C_{self} of an isolated spherical nanoparticle (NP) (radius r_{NP} = 10 nm, near SiO_2, ε_r= 3.9) is given by $C_{self} = 4\pi\varepsilon_0\varepsilon_r r_{NP}$ = 3.9 aF. The mutual-capacitance C_m between adjacent NPs separated by molecular barriers (1-octanethiols, ε_r = 2.6) of width d (1 nm) << r_{NP} is given by $C_m = 4\pi\varepsilon_0\varepsilon_r r^2_{NP}/(2r_{NP}+d)$ = 1.3 aF. Assuming 9 nearest neighbours around an NP (at the base of close-packing structure), its total capacitance $C_0 = C_{self} + 9\ C_m$ = 15.6 aF. Hence, its charging energy $E_c = e^2/C_0$ = 10 meV. For a single NP, the voltage threshold where it is in an OFF-state is given by $eV_0 = E_c$, i.e. V_0 = 10 mV. When the thermal energy broadening 3.5 k_BT is comparable to 10 meV (T~30 K), we completely lose nonlinear switching behaviour. In fact, we experimentally observe (Supplementary Fig. S1) that Coulomb blockade is incomplete even at 5 K.

Resistance due to the molecular barrier

The ON-state resistance R_0 of a single NP is determined by the ~1 nm thick 1-octanethiol layer covering it. For further analysis, we assume that all NPs participating in electron transport have a resistance much larger than the quantum resistance. i.e. $R_0 >> h/e^2$ = 25.8 kΩ.

Nanoparticle cluster estimation

Here we estimate the size, shape and interconnectivity of the NP clusters (i.e. subsets of the total NP network) that are involved in electron transport between a pair of electrodes. For any NP cluster, the voltage threshold V_{th} depends only on the smallest number of NPs connecting both electrodes. This is defined as the cluster size n. In contrast, the total resistance R_{tot} of a cluster

DOI: 10.1038/NNANO.2015.207

depends on its shape (dimensionality) and connectivity (number of nearest neighbours). Assuming a regular connectivity, Table S6a lists these scaling rules with respect to the dimensionality. Note that the power dissipated (last column of Table S6a) is an extrinsic quantity proportional to N, the total number of nanoparticles involved. In Fig. S6, we estimate that in total around 10-100 NPs participate in electron transport between various pairs of electrodes. The maximum cluster size is ~10, expected for diametrically opposite electrodes separated by 200 nm and connected by 20 nm particles. We also find clusters with R_{tot} even lower than those of a 3D block. Such "hyperconnected" clusters (exhibiting a large number of nearest neighbours) may have much more than 8 participating nearest neighbours on average.

Conductance modulation via back-gate potential

The dependence of the output current (I_{OUT}) on the static control voltages applied to the metal electrodes, described in the Letter provides one means of control over the potential landscape. In addition to this, another (global) control is used in the form of the back-gate voltage ($V_{bg} \equiv V_6$) applied to the p++ doped Si substrate. With application of a fixed source-drain voltage (V_{sd}) between two electrodes (one of which being GND), the conductance can be modulated by varying V_{bg} relative to GND. In Fig. S1e, a 2D colour scale plot of $\log|I_{OUT}|$ versus (V_{sd}, V_{bg}) clearly shows the conductance modulation, which suggests superposition of multiple open Coulomb diamonds. This is expected, as successful conduction across the 200 nm gap between diametrically opposite electrodes requires a minimum of 10 participating NPs. Moreover, being a global gate, application of V_{bg} as the 6th control voltage (V_6) strongly influences the logic output, as seen in Fig. S7.

S2. Robustness of the device functionality

Sensitivity vs. direction and logic

The robustness of a genome's performance to voltage fluctuations may be characterized by the variation in the fitness landscape. However, exhaustively characterizing this variation in a 6-dimensional variable space is time consuming. We need an algorithm that (1) samples the space such that it captures the regions of interest, (2) predicts outcomes by weighing in observations from crucial nearest neighbours.

If our goal is to estimate the robustness of the fittest genome G_α, it is crucial to sample more genomes with fitness near F_α. And this is what a GA search does, naturally! So, we take those genomes and predict the fitness landscape by calculating a random forests regression[1]. This technique is well suited, as the shape of the neighbourhood used by a random forest adapts to the local importance of each variable (i.e. gene). In Fig. S7a, we see that for perturbations local to G_α, the fitness decreases with increasing distance. The decay rate of predicted fitness also depends substantially on the perturbation direction.

In Fig. S7b, we again see that the fitness is more sensitive to variations along certain directions, e.g. the fitness of G_α for an AND is sensitive to a negative perturbation in gene g_3, whereas being insensitive to a positive perturbation. In case of an XOR, we see that the fitness is sharply sensitive to gene g_6 in both directions. This implies that conventional hill-climbing algorithms are indeed unsuitable to find such logic gates.

Temperature fidelity and gate interchangeability

To illustrate the temperature fidelity and gate interchangeability of the solutions, the inverter ($\bar{P}$) and AND ($P{\cdot}Q$) gates were applied alternately, and the output was recorded during warming up to 15 K and cooling down to base temperatures (0.28 K). In Fig. S9 shows the variation of the fitness with temperatures and signal response of these two gates. The temperature was ramped up and post settling time of 2 minutes at each temperature step, AND ($P{\cdot}Q$) and inverter ($\bar{P}$) were sampled multiple times. The average fitness from 30 measurements is plotted with T in Fig. S9. This shows that the gate responses are independent of thermal-cycling (to 15 K) and also can be set interchangeably. As shown in inset panels, at higher temperatures, the response resembles the behaviour from a network of linear resistors and hence acts like a simple voltage divider. The inverter response from Fig. 3c is also reproduced here for comparison.

S3. Evidence for advanced functionality

Our system meets the generally accepted four criteria to be a suitable building block (or "cell") for the physical realization of a neural network, in particular for implementing a cellular neural network (CNN[2]) universal machine. A CNN is like a neural network, but with only nearest-neighbour interactions between the cells, and therefore much easier to practically implement, but

DOI: 10.1038/NNANO.2015.207

with maintaining the same power as a general neural network for solving more complex problems[3].

These four criteria are [4, pg. 24-26]:

- **Universality**: the possibility to use the same physical structure of the CNN cell for implementing arbitrary Boolean functions, by simply changing (programming) the cell parameter values. This is exactly what we show in our system by the reconfigurability of one and the same network into all Boolean logic gates by evolutionarily adjusting the control voltages!
- **Compactness**: only a small set of control parameters is needed to satisfy universality. We only use six control voltages to realize all Boolean logic (in fact all 16 possible 2-input-1-output truth tables). The necessary area (200 nm diameter) is competitive with state-of-the-art CMOS technology for the same functionality.
- **Robustness**: the functionality must be robust against fluctuations in the control parameters. We elaborately discuss the robustness of our system against control voltage fluctuations, under thermal cycling, and as a function of time.
- **Evolvability**: the capability of a system to be evolved into a desired functionality. We clearly demonstrate this in our nanomaterials system by utilizing a genetic algorithm.

The fact that our system meets all the above criteria directly implies the applicability of our approach for realizing complex functionality beyond Boolean logic by upscaling the present architecture and using more complex electrode geometries.

S4. Advantage over existing parallel architectures

Our device is functionally robust (although it is assembled out of charge sensitive nanoparticles) as it is evolved over an interconnected network, where redundancy and parallelism provide for fault-tolerance and efficiency. Redundancy is known[5,6] to tackle challenges of imprecise fabrication in further scaling down of nanoelectronics. Parallelism is known[7] to achieve brain-like efficiency.

But existing architectures are still made out of CMOS based components. While such well-defined components were necessary to implement conventional programming languages, we are now at the cusp of an AI boom; several difficult problems like pattern recognition are being more efficiently solved by evolutionary algorithms on artificial neural networks. As discussed in

section S3, our nanoparticle networks can be scaled up and evolved to function as a CNN. Our evolutionary approach is both fault-tolerant and can exploit all physical processes at hand, like cross-talk among neighbouring cells (that are usually seen as a design restriction). This makes natural computers in general much more efficient in terms of space occupied and energy consumed.

DOI: 10.1038/NNANO.2015.207

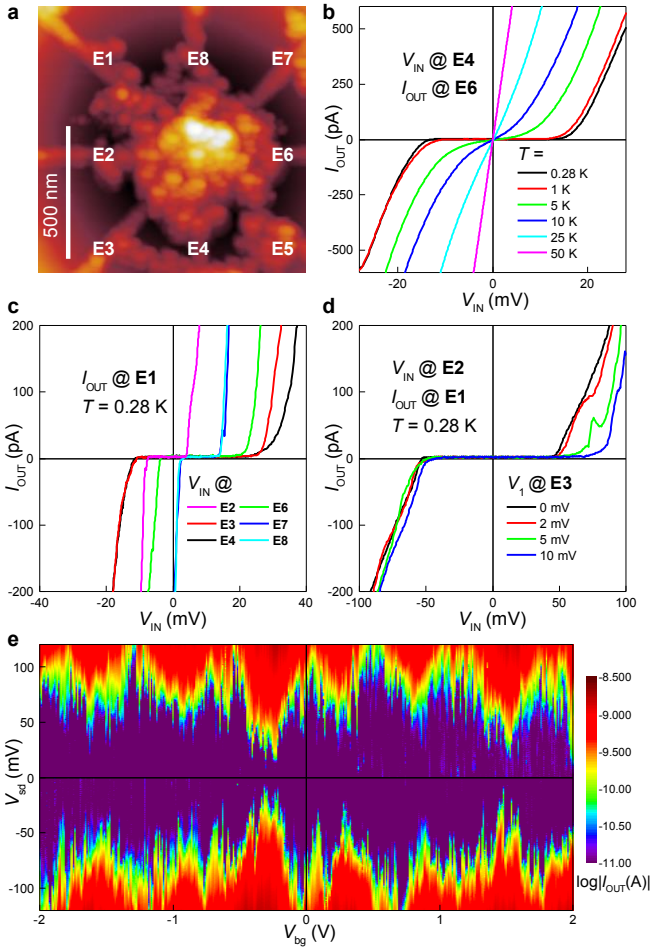

Supplementary Fig. S1| Modulation of Coulomb blockade in NP network: a, Atomic force micrograph of Au NP network with electrodes numbered E1-E8. The electron transport below ~5 K is dominated by Coulomb blockade, and strongly depends on the used input and output electrodes, as well as on the static voltages applied to the remaining electrodes. This is indicated by dependence of I_{OUT}-V_{IN} characteristics on: **b,** operating temperature, **c,** position of input electrode, **d,** applied voltage on remaining electrode. **e,** Typical conductance between a pair of electrodes (V_{sd} vs. I_{OUT}) of the NP network as a function of the back-gate voltage V_{bg}.

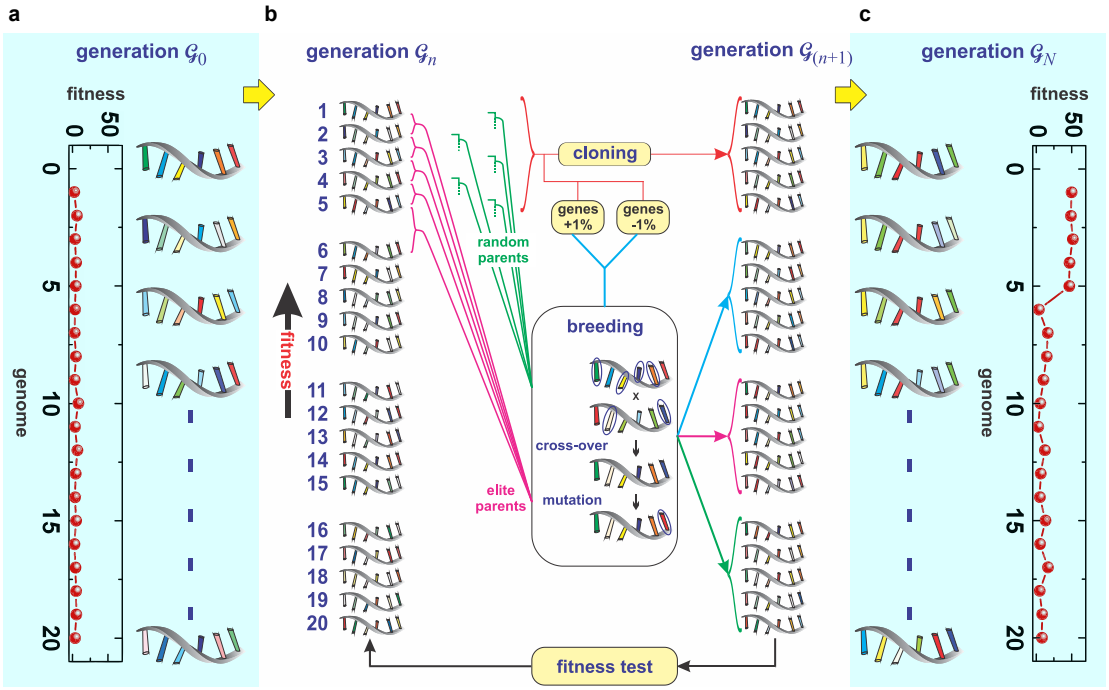

Supplementary Fig. S2| GA schematic: a, A genetic algorithm searches for optimum genomes by iterating over generations. Every generation $\mathcal{G}_n$, has a fixed population of 20 genomes (represented by strands) that are each composed of six genes (control voltages $V_{1..6,}$ represented by coloured bars). The GA starts with a random initial generation $\mathcal{G}_0$, whose fitness is generally low, as indicated here (GA search for AND gate). **b,** With a composite cloning-breeding procedure (see Methods) for evolving generation $\mathcal{G}_n$ into $\mathcal{G}_{(n+1)}$, we eventually reach **c,** a final generation $\mathcal{G}_N$ whose top genomes have higher fitness than corresponding to $\mathcal{G}_0$.

DOI: 10.1038/NNANO.2015.207

a

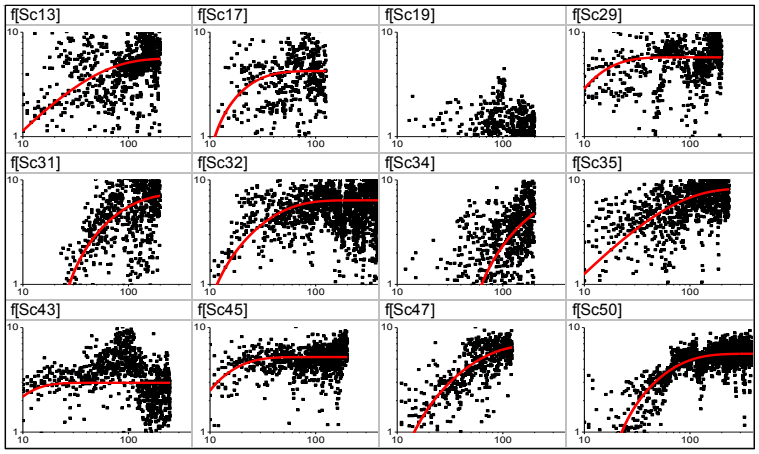

b

	F_0	n_0
f[Sc13]	5.6	94
f[Sc17]	4.2	35
f[Sc19]	0.9	80
f[Sc29]	5.7	23
f[Sc31]	7.4	153
f[Sc32]	6.4	69
f[Sc34]	7.9	435
f[Sc35]	8.3	135
f[Sc43]	3	14
f[Sc45]	5.2	24
f[Sc47]	6.9	104
f[Sc50]	5.6	112

c

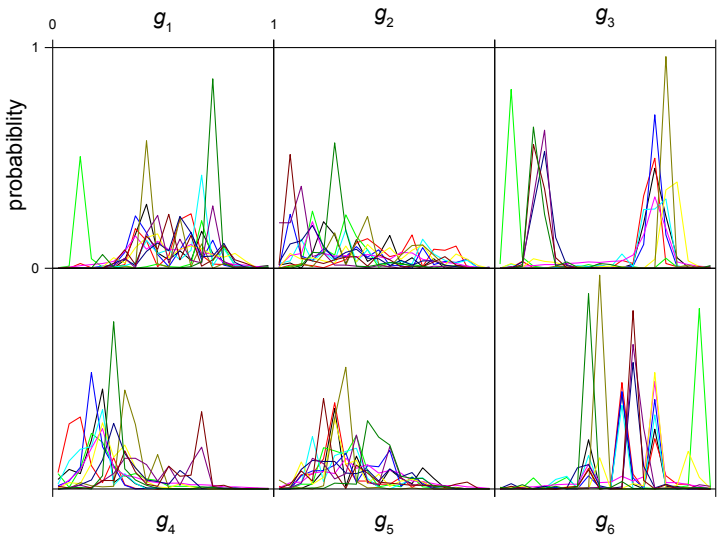

Supplementary Fig. S3| GA convergence. a, We scatter plot $F(G_{n,i})$ vs. n, i.e. fitness scores of the cloned genomes (i = 1,2,...5) in every generation, for multiple re-runs of GA search for a NAND. f[Sc#] corresponds to the fitness scatter of search Sc#. The numbers # are not contiguous as the NAND searches were interspersed with searches for other gate types and thermal cycles, over a period of two weeks. The red line is an asymptotic fit from which we obtain a stable score F_0 and convergence generation n_0. Despite the time-dependent stochasticity, the GA preserves robust solutions (See Fig. S9). **b,** If we define $F_0 > 2$ as criterion for success, we see that this GA search converged in 11 out of 12 identical cases. We see that n_0 has a median value of ~90 generations = 1800 genomes = 40 minutes of experimental measurements. **c,** We plot a histogram (20 bins) of the experimental probability of genes explored for multiple re-runs (distinguished by colors) of a GA search for NAND. The genes ($g_1 - g_6$) have an affinity towards certain desirable values, and this is especially striking in g_3 and g_6. Note that g_3

determines the voltage applied on an electrode adjacent to I_{OUT}, whereas g_6 determines the global back-gate voltage.

P	Q	NOT P	NOT Q	AND	OR	NAND	NOR	XOR	XNOR
1	1	0	0	1	1	0	0	0	1
1	0	0	1	0	1	1	0	1	0
0	1	1	0	0	1	1	0	1	0
0	0	1	1	0	0	1	1	0	1

Supplementary Fig. S4| Boolean Logic. Truth table covering basic Boolean logic combinations for two inputs *P* and *Q*.

DOI: 10.1038/NNANO.2015.207

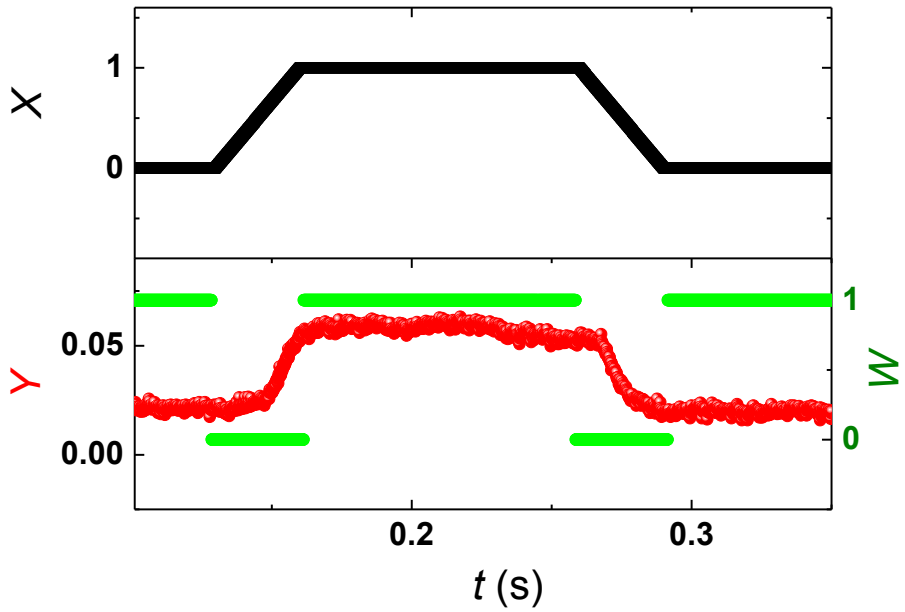

Supplementary Fig. S5| Evaluating output. The measured output *Y* (red symbols in lower panel) is fit to an ideal output *X* (upper panel). During logic transitions, indicated by shaded regions, the weights *W* are set to 0, and thus the measurements are neglected. For detailed fitting procedure please refer to Methods.

a

Dimensionality	Connectivity	V_{th}	R_{tot}	Power Dissipation V^2_{th}/R_{tot} $(= NV^2_0/R_0)$
1D (n chain)	2	nV_0	nR_0	nV^2_0/R_0
2D ($n\times n$ sheet)	4	nV_0	R_0	$n^2V^2_0/R_0$
3D ($n\times n\times n$ block)	6	nV_0	R_0/n	$n^3V^2_0/R_0$

b

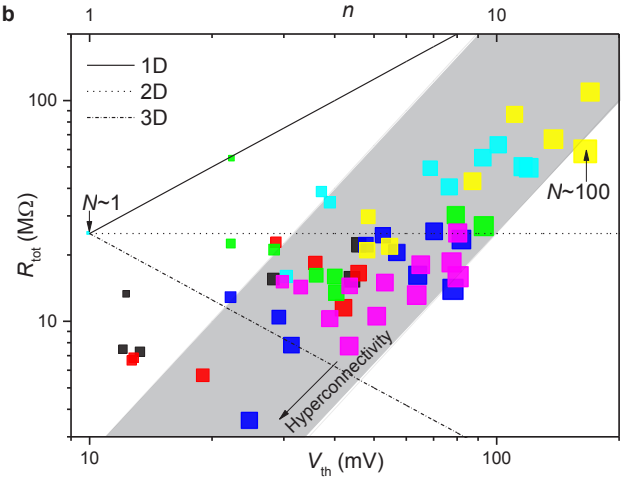

Supplementary Fig. S6| Cluster shape and size. a, Table listing cluster scaling rules. **b,** For various pairs of electrodes among different samples (distinguished by colors), we plot a square at the experimentally measured (V_{th},R_{tot}). The size of the square represents the total number of NPs involved, estimated (using last column of table) as $N = (V^2_{th}/R_{tot})/(V^2_0/R_0)$. Sample cyan contains the smallest cluster size n~1 (also N~1). From its resistance, we estimate $R_0 = 25$ MΩ. The solid, dashed and dashed-dot lines indicate the dimensionality. We estimate that most electrode pairs have between 10-100 NPs participating in electron transport in between them, indicated by the grey shaded region. Clusters with very low R_{tot} are expected to be "hyperconnected" (i.e. exhibiting a large number of nearest neighbors).

DOI: 10.1038/NNANO.2015.207

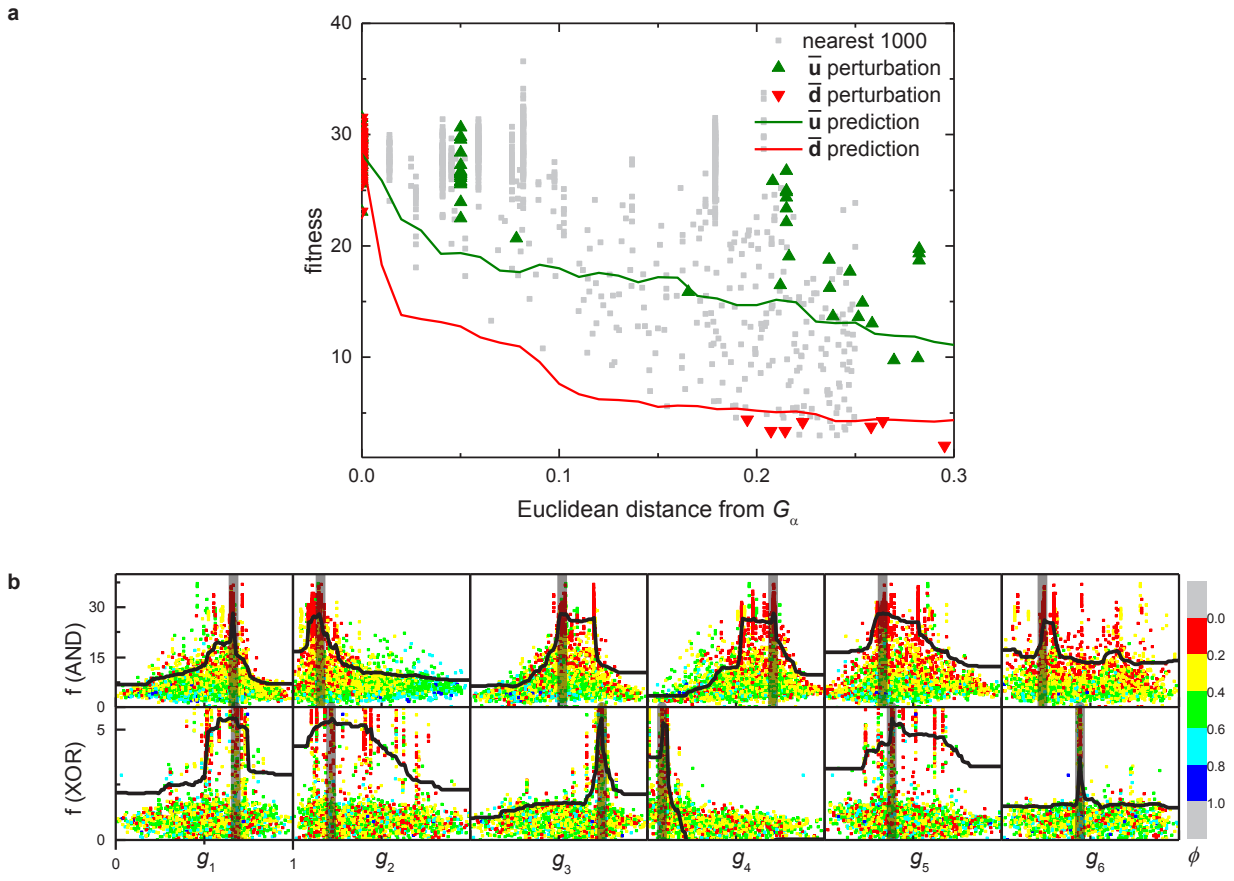

Supplementary Fig. S7| Fitness sensitivity. a, Sensitivity versus perturbation direction**:** For a GA-searched AND, we plot the fitness of genomes explored near the fittest genome G_α = (0.66,0.16,0.52,0.71,0.33,0.23). The green/red triangles correspond to genomes perturbed along (angular deviation less than 0.5) the direction $\bar{u}$(0.03,0.06,0.13,-0.79,0.59,-0.06)/ $\bar{d}$(0.92,-0.08,-0.36,0.05,0.00,0.08). The solid lines are predictions made by a random forest regression[1] for fitness variation exactly along a perturbation direction. **b,** Sensitivity versus logic**:** For GA searches AND/XOR, we study the fitness variation of G_α to perturbations along the coordinate axis g_i, i = 1:6. The unperturbed coordinates of G_α are marked by the transparent black strips. The explored genomes are scatter plotted with a color indicating their angular deviation (ϕ) from a 1D perturbation along each coordinate axis, i.e. red genomes are near-exact perturbations along the corresponding coordinate axis. The solid black line is a prediction made by a random forest regression for fitness variation exactly along each coordinate axis.

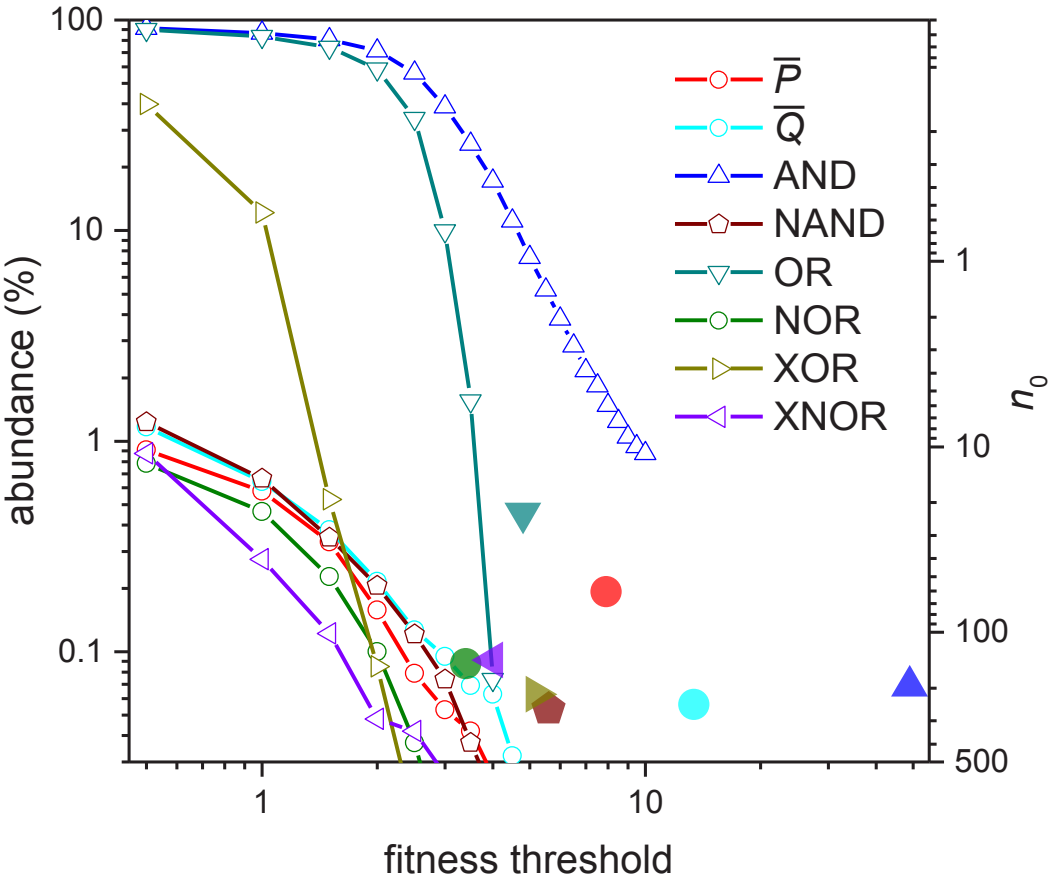

Supplementary Fig. S8| GA merits. A GA is considered successful if it helps in discovering fitter genomes faster than a random search. For this, we compare the abundance of a random search (Fig. 2e) with an equivalent metric for the GA (i.e. a fitness threshold = F_0 with abundance = $100/20n_0$). The solid symbols are the abundance metric for GA searches (corresponding to Fig. 2e) and it demonstrates the improvement in abundance and fitness due to GA.

DOI: 10.1038/NNANO.2015.207

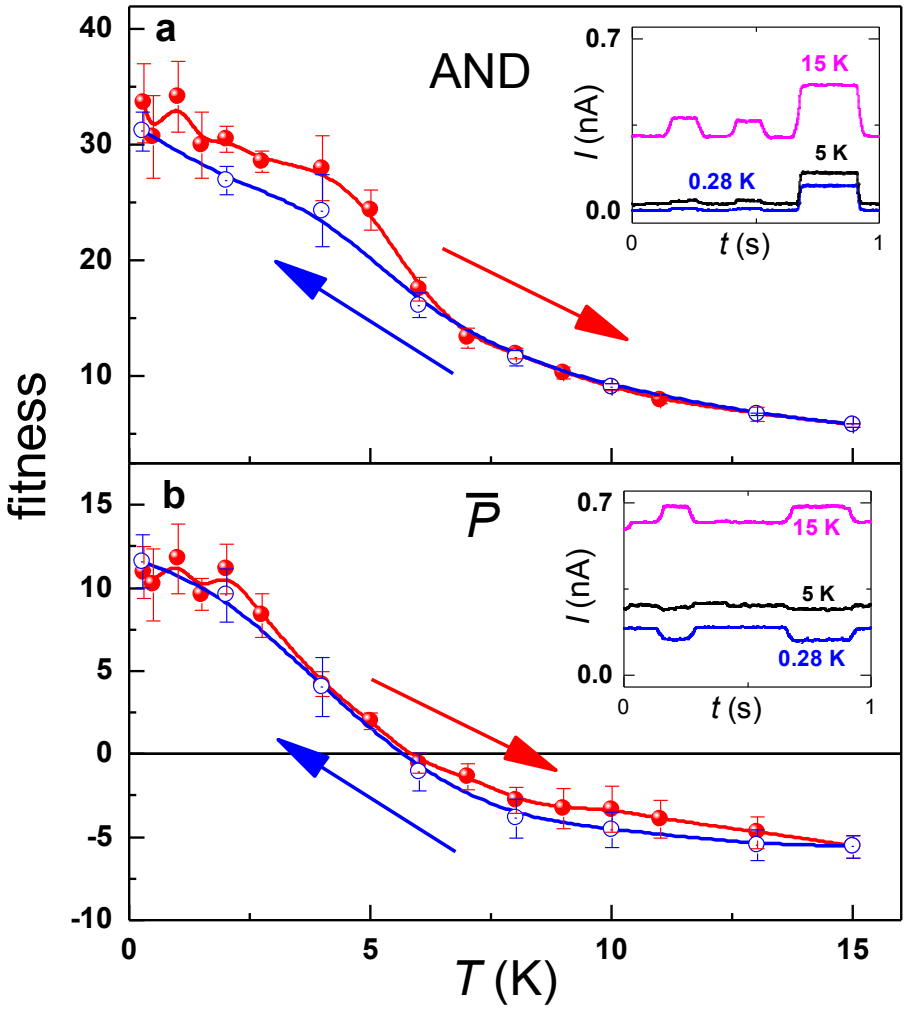

Supplementary Fig. S9| Robustness to thermal cycling. a-b, Temperature fidelity tests for $\bar{P}$ and AND ($P{\cdot}Q$) for both forward and reverse sweeps, confirming the stability of the gate solution for $T < 5\ K$. The output response loses the gate behavior at higher temperatures as shown in the corresponding insets. The data for $\bar{P}$ are reproduced here from Fig. 3c.

References

1. Lin, Y. & Jeon, Y. Random forests and adaptive nearest neighbors. *J. Am. Stat. Assoc.* **101**, 578-590 (2006).
2. Roska, T. & Chua, L. O. The CNN Universal Machine: An Analogic Array Computer. *IEEE Trans. on Circuits and Systems-II* **40**, 163-173, (1993).
3. Roska, T. Cellular wave computers for brain-like spatial-temporal sensory computing. *Circuits and Systems Magazine, IEEE* **5**, 5-19, (2005).
4. Dogaru, R. *Universality and emergent computation in cellular neural networks*. Vol. 43 (World Scientific, 2003).
5. Heath, J. R., Kuekes, P. J., Snider, G. S. & Williams, R. S. A defect-tolerant computer architecture: opportunities for nanotechnology. *Science* **280,** 1716–1721 (1998).
6. Snider, G. S. & Williams, R. S. Nano/CMOS architectures using a field-programmable nanowire interconnect. *Nanotechnology* **18,** 1–11 (2007).
7. Merolla, Paul A., *et al*. A million spiking-neuron integrated circuit with a scalable communication network and interface. *Science* **345**, 668-673, (2014).